BioNanoScience (2020) 10:1037–1048
https://doi.org/10.1007/s12668-020-00775-5

Antibacterial Studies of ZnO and Cu-Doped ZnO Nanoparticles Synthesized Using Aqueous Leaf Extract of *Stachytarpheta jamaicensis*

Mohammad Mansoob Khan[1] · Mohammad Hilni Harunsani[1] · Ai Ling Tan[1] · Mirabbos Hojamberdiev[2] · Yap Ai Poi[3] · Norhayati Ahmad[3]

Published online: 22 July 2020

Abstract
Zinc oxide (ZnO) and Cu-doped ZnO nanoparticles (1% and 5%; Cu-doped ZnO NPs) were synthesized using aqueous leaf extract of *Stachytarpheta jamaicensis*. Crystalline ZnO and Cu-doped ZnO NPs with hexagonal wurtzite structure were obtained without any impurities as confirmed by powder X-ray diffraction. The optical properties, morphology, elemental composition, and surface analysis of all the samples were studied using UV-vis diffuse reflectance spectroscopy, scanning electron microscopy equipped with energy dispersive X-ray analysis (SEM-EDX), and X-ray photoelectron spectroscopy, respectively. Antibacterial activities of the ZnO and Cu-doped ZnO were performed by screening test at the highest concentration (500 mg/mL) against two gram-positive bacterial strains (*Bacillus subtilis* and *Staphylococcus aureus*) and two gram-negative bacterial strains (*Pseudomonas aeruginosa* and *Escherichia coli*). Antibacterial activities were observed only against gram-positive bacteria. Minimum inhibitory concentration (MIC) ranged from < 25 to 50 mg/mL.

Keywords Zinc oxide (ZnO) · Cu-doped ZnO · Green synthesis · Aqueous leaf extract · *Stachytarpheta jamaicensis* · Antibacterial activities

1 Introduction

Zinc oxide nanoparticles (ZnO NPs) are a member of the group II-VI semiconductor with a wide and direct band gap (~ 3.2 eV) at room temperature that mainly crystallizes in the wurtzite structure with broad applications [1, 2]. ZnO NPs can be synthesized through several ways such as chemical method—sol-gel synthesis and solvothermal synthesis; physical method—evaporation-condensation and pulse laser ablation as well as biological methods that involve the use of plant or microorganisms [3, 4]. Microbial synthesis of the ZnO NPs using microorganisms such as bacteria, fungi, and yeast involves multiple purification steps and further additional steps to maintain the cell cultures and intracellular synthesis. Hence, green synthesized ZnO NPs using plant extract seem more stable and faster than other biosynthesized NPs which involved microorganisms [5].

Unlike green synthesis, chemical methods may involve the use of certain toxic reducing agents or/and solvents that may have harmful effects to human beings such as causing irritation to the skin, eyes, and ear, as well as causing environmental toxicity. Some chemical reaction might lead to the presence of toxic chemical species adsorbed on the surface of the NPs that may have adverse effect in medical application [6]. For physical methods, they tend to have a high-cost, high energy consumption but low product efficiency and also require conditions such as high pressure and temperature. Compared with chemically synthesized ZnO NPs, green synthesized ZnO NPs showed a better bactericidal activity against various pathogens. Hence, green synthesis of metal oxide NPs has increasingly become the subject of interest among the scientific community [7].

Green synthesis has the advantage of being non-toxic and biocompatible. The process mainly uses water as the solvent

✉ Mohammad Mansoob Khan
mmansoobkhan@yahoo.com; mansoob.khan@ubd.edu.bn

[1] Chemical Sciences, Faculty of Science, Universiti Brunei Darussalam, Jalan Tungku Link, Gadong, BE 1410, Brunei Darussalam

[2] Institut für Chemie, Technische Universität Berlin, Straße des 17, Juni 135, 10623 Berlin, Germany

[3] Environmental and Life Sciences, Faculty of Science, Universiti Brunei Darussalam, Jalan Tungku Link, Gadong, BE 1410, Brunei Darussalam

and does not require the use of toxic chemicals such as strong reducing agents and corrosives. [8]. Thus, this makes the green synthesis a potential commercial alternative for large-scale production. NPs that are produced by plants are more stable and can have various controlled shapes and sizes [9]. Numerous active biomolecules of the plant coated on the surface of the NPs allow multiple ligand–based conjugation of nanoparticle with receptors on bacterial membranes [8]. These bioactive components present in *Stachytarpheta jamaicensis* leaves extract also play a crucial role in the NP synthesis as they act as capping agents that efficiently stabilize the formation of ZnO NPs for different biological application [10]. Native to Northern South America and Central America, *S. jamaicensis* (Fig. 1) is a flowering plant with a blue to purple flower under the family Verbenaceae. *S. jamaicensis* is used to treat infectious diseases and wounds based on its traditional usage. The crude plant extracts of the leaf, stem, and root of the plants have been reported to exhibit antimicrobial and antifungal activity [11].

The plant can be used to treat diabetes [12], diarrhea, and headaches [11]. Meanwhile, macerated leaves can be used for treating external ulcer [11] and wounds [13]. It can also be used to treat allergies and respiratory diseases such as cold, asthma, and flu as well as various digestive problems like indigestion, constipation, and acid reflux [11]. The plant has been reported to contain various types of phytochemicals such as alkaloids, saponins, tannins, flavonoids, and phenolic compounds that served as a defense mechanism against invasion by many microorganisms [14]. Murugan et al. reported that tannins can inhibit the growth of microorganisms by impeding the protein synthesis via the binding to the proline rich proteins, while saponins are the antifungal agents that can cause outflow of proteins and certain enzymes from the cell [15]. Upon the invasion of pathogens, the plant will synthesize flavonoids which are a hydroxylated phenolic substance that can kill numerous bacterial strains and also some viral enzymes.

Fig. 1 Leaf and flower of *Stachytarpheta jamaicensis*

The phytochemicals found in the medicinal plant itself cannot fully kill bacteria as some of the bacteria might have developed resistance towards them. Thus, certain modifications are needed to improve the bactericidal effect of the bioactive molecules which includes the metal oxide NPs synthesized using the leaves extract and water as the solvent. These metal oxide NPs with sizes less than 100 nm are small enough to penetrate through the membrane lipid of the bacteria cell membrane. The size of the holes of the gram-positive bacteria cell wall is predicted to be 15–24 nm [16]. Several types of metal oxide NPs are proven to have antibacterial properties such as CuO, Fe_2O_3, ZnO, Ag_2O, SiO, CuO, ZnO, TiO_2, MgO, and CaO NPs [7–9, 17]. Among metal oxides, ZnO NPs possess a large surface area to volume ratio which can dramatically increase the bactericidal effectiveness [8].

ZnO NPs is one of the components found in antibacterial ointment due to its antimicrobial and antibacterial properties. Gram-positive bacteria have many layers of peptidoglycan ranging in thickness from 30 to 100 nm thick [18]. On the other hand, the gram-negative bacteria have only three layers of peptidoglycan with thickness of a few nanometers. Teichoic acid and lipoteichoic acid are present in the gram-positive bacteria only (Fig. 2). The presence of these acids maintains the rigidity of the cell [8], chelate the Zn^{2+} ions from ZnO NPs, and transport the ions into the cell. Porin, an ion channel which aids the passive diffusion of NPs into the cytoplasm of cells, is found in the outer layer of the peptidoglycan [8]. Apart from that, ZnO NPs can also enter the cell through endocytosis.

Copper (Cu) was selected as the dopant for ZnO since it is a transition metal with similar ionic radii (71 pm) to Zn (74 pm) [19]. Cu doping can also alter the optical properties of the ZnO system such as band-gap reduction [20] and shifting of absorption into longer wavelength [21]. Incorporation of Cu atoms into the lattices of ZnO nanostructures has been shown to modify the morphology of ZnO nanostructures [22]. Doping ZnO NPs with other metals such as gold, silver, copper, and magnesium can enhance the antimicrobial activity of the ZnO NPs itself. Cu-doped ZnO NPs showed a greater bactericidal activity and larger diameter of the inhibition zone on the bacterial growth when tested against both gram-positive and gram-negative bacterial strains when compared with pure ZnO NPs [23, 24].

The aim of this study is to synthesize ZnO NPs and 1% and 5% Cu-doped ZnO NPs using aqueous leaves extract of *S. jamaicensis* via green synthesis, which is a low cost and an eco-friendly method, and study their antibacterial properties. The synthesized ZnO NPs and Cu-doped ZnO NPs were characterized using different sophisticated techniques and tested against both gram-positive (*Bacillus subtilis* and *Staphylococcus aureus*) and gram-negative bacteria (*Pseudomonas aeruginosa* and *Escherichia coli*) to investigate the antibacterial activities.

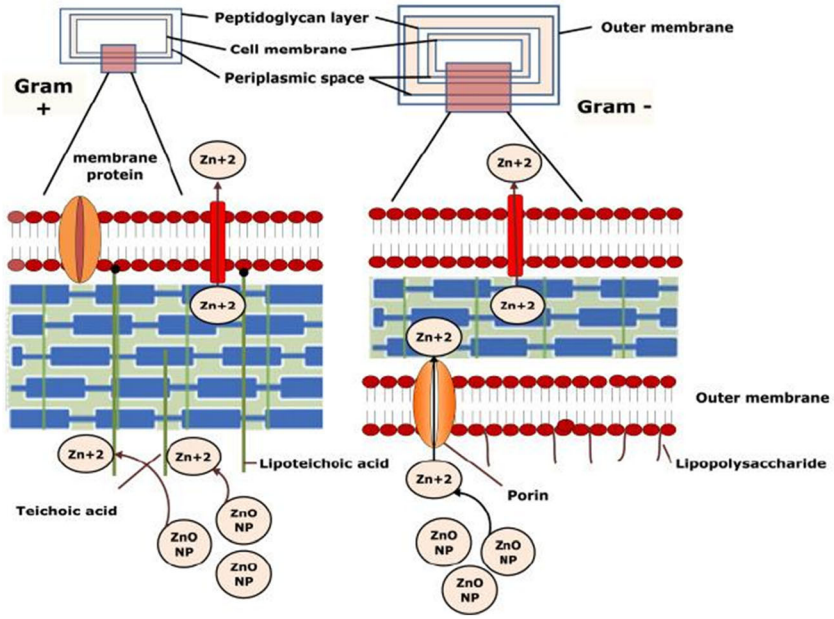

Fig. 2 Attachment of ZnO NPs at gram-positive and gram-negative bacteria [8]

2 Methodology

2.1 Materials Used

Zinc nitrate hexahydrate ($Zn(NO_3)_2{\cdot}6H_2O$) and copper chloride dihydrate ($CuCl_2{\cdot}2H_2O$) were purchased from Sigma-Aldrich. Four different bacterial strains were used to perform the antibacterial activity namely, two gram-positive bacteria: *Bacillus subtilis* (*B. subtilis*; ATCC6833) and *Staphylococcus aureus* (*S. aureus*; ATCC25923) and two gram-negative *Escherichia coli* (*E. coli*; ATCC25922) and *Pseudomonas aeruginosa* (*P. aeruginosa*; ATCC27853). Mueller-Hinton Agar (MHA) powder and nutrient broth powder was purchased from Sigma-Aldrich.

2.2 Collection of the Plant Leaves

The leaves of *S. jamaicensis* (family: Verbenaceae) was collected within the Universiti Brunei Darussalam (UBD) campus and the species were confirmed by a botanist at the UBD Botanical Research Centre.

2.3 Preparation of Aqueous Leaf Extract

The leaves of *S. jamaicensis* plant were washed several times to remove dust on the surface of the leaves. The leaves were air dried overnight at room temperature before being cut and ground into fine pieces using a blender. Subsequently, 100 mL of distilled water was then added to a 5 g portion of the blended leaves. The mixture was then left to stir at room temperature for 1 h using a magnetic stirrer. The leaf suspension was gravity filtered through Whatman No.1 filter paper and the aqueous leaf extract/filtrate was collected in a conical flask.

2.4 Synthesis of Undoped Zinc Oxide Nanoparticles

$Zn(NO_3)_2{\cdot}6H_2O$ (3 g, 0.01 mol) was added into the aqueous leaf extract (30 mL) and the mixture was heated to 60 °C. A brown paste was obtained which was then calcined in a muffle furnace at 400 °C for 2 h. The light yellow ZnO NP fine powder product obtained was ground to much finer form by using pestle and mortar for further characterization and analysis.

2.5 Synthesis of 1% and 5% Cu-Doped ZnO NPs

Cu-doped ZnO NPs were synthesized using the same procedure as section 2.4, using the same amount of leaves (5 g) and $Zn(NO_3)_2{\cdot}6H_2O$ but with an addition of $CuCl_2{\cdot}2H_2O$ as dopant. Both $Zn(NO_3)_2{\cdot}6H_2O$ and $CuCl_2{\cdot}2H_2O$ were added simultaneously into the hot leaf extract at 60 °C. Two different Cu-doped ZnO NPs were synthesized, i.e., 1% Cu-doped ZnO and 5% Cu-doped ZnO NPs under the same conditions.

2.6 Characterization of Nanoparticles

The synthesized ZnO NPs and Cu-doped ZnO NPs were characterized using different techniques. The synthesized nanomaterials were analyzed using powder X-ray diffraction (XRD) (MiniFlex II from Rigaku, Japan) where Cu Kα radiation was used with wavelength (λ) of 0.15418 nm to determine purity of samples and crystallite size [3, 4]. For optical properties, diffuse reflectance spectroscopy (DRS, UV-3600 UV-Vis-NIR spectrophotometer, Shimadzu, Japan) was performed for the determination of band gap energy [3, 4]. Characterization by scanning electron microscopy and energy dispersive X-ray analysis (SEM and EDX; JSM-7600F field-

emission-type scanning electron microscope from JEOL, Japan) was done for determining the particles size, morphology, and elemental composition. X-ray photoelectron spectroscopy (XPS; JPS-9010MC, JEOL, Japan) was used to investigate the surface elemental composition and binding state. The zeta potential analysis was performed (Malvern Zetasizer, Nano series) to determine the surface net charge.

2.7 Antibacterial Screening

The samples were first screened for antibacterial activity at the highest concentration of 500 mg/mL using the Kirby-Bauer disc diffusion method [25]. A 500 mg/mL suspension of ZnO was prepared by adding 0.5 mL distilled water to 0.25 g of undoped ZnO NPs followed by sonication. A 10 μL of suspension was added onto a 5 mm disc of Whatman No.1 filter paper. The procedure was repeated for the 1% Cu-doped ZnO and 5% Cu-doped ZnO NPs. A disc added with 5 μL of 20 mg/mL streptomycin and another disc with distilled water were used as positive and negative controls, respectively. Additionally, a 500 mg/mL commercial ZnO (C-ZnO) NP suspension was also prepared by using the same method to act as a second positive control for screening test. All the impregnated discs were dried overnight.

The bacterial strain was first grown in nutrient broth and was incubated at 37 °C for 24 h. The turbidity of the final nutrient broth was adjusted to achieve an absorbance of 0.07–0.1 equivalence to the absorbance of 0.5% barium sulfate solution. The bacterial lawn was then spread over a Mueller-Hinton agar (MHA) plate. Each MHA plate was divided into six sections, with the respective label. A sterilized tweezers was used to place the impregnated discs onto its allocated section on the MHA plate and the negative control disc was placed in the middle of the plate. The MHA plate was then incubated at 37 °C for 24 h. These steps were repeated for the other three bacterial strains and the screening test was repeated three times for each bacterial strain. The mean diameter of the zone of inhibition and its standard deviation (± SD) were measured and recorded.

2.8 Minimum Inhibitory Concentration

The NP's that showed significant zone of inhibition were further analyzed using the Kirby-Bauer disc diffusion method in order to determine the lowest concentration that inhibits the microbial growth after 24 h incubation [25]. A 500 mg/mL suspension of the undoped ZnO NPs was serially diluted to achieve the working concentrations of 250 mg/mL, 100 mg/mL, 50 mg/mL, and 25 mg/mL, with streptomycin (20 mg/mL) used as the positive control and distilled water as the negative control. Seven sterile discs at 5 mm diameter were prepared and each of them was impregnated with 10 μL of the different concentrations of the NPs suspensions.

The MHA plate with the bacterial lawn was divided into six sections where each disc was placed in its own individual labeled section. The MHA plate was then incubated overnight at 37 °C and the zone of inhibition of each disc was measured. These steps were carried out in triplicates (for each bacterial strains tested) for each of the compounds and the mean diameter of the zone of inhibition was measured and recorded.

3 Results and Discussion

3.1 ZnO and Cu-Doped ZnO NP Synthesis

Green synthesis method was adopted to fabricate the ZnO, 1%, and 5% Cu-doped ZnO using the aqueous leaf extract of *S. jamaicensis*. The advantage of this method is that it is simple, green, environment friendly and provides additional capping and reducing agents, because plant extract contains

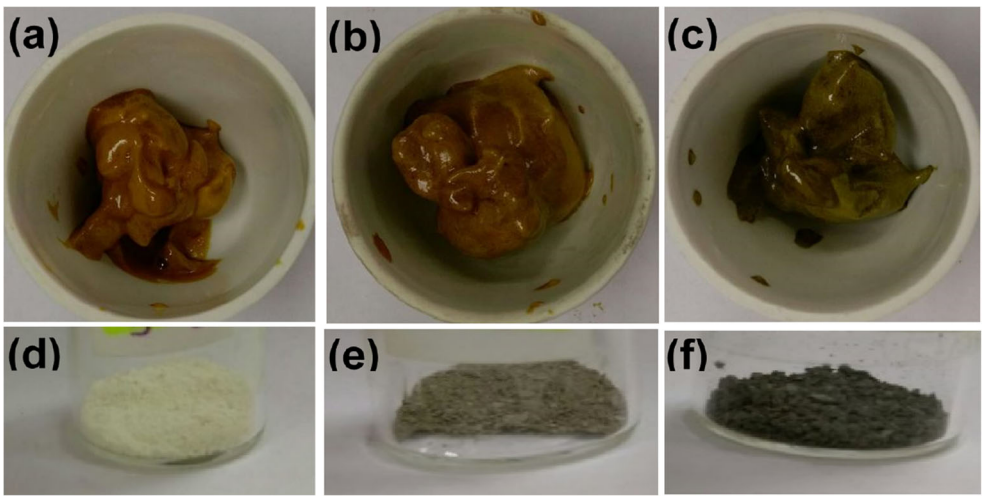

Fig. 3 Paste formed at the end of heating reaction mixture for (**a**) undoped ZnO, (**b**) 1% Cu-doped ZnO, and (**c**) 5% Cu-doped ZnO. The ZnO NP powder formed after calcination (**d**) undoped ZnO, (**e**) 1% Cu-doped ZnO, and (**f**) 5% Cu-doped ZnO NPs

variety of biomolecules, which function as capping and reducing/oxidizing agents during NP synthesis.

The solvent used was water and the synthesis process takes place at low temperature, 30–60 °C, except calcination of the paste at 400 °C. The paste formed (Fig. 3) after heating was brown for both undoped ZnO NPs (Fig. 3a) and 1% Cu-doped ZnO (Fig. 3b) while for 5% Cu-doped ZnO, the paste was dark green (Fig. 3c). Following calcination, the paste for undoped ZnO NPs turned into a light yellow powder (Fig. 3d). The 1% Cu-doped ZnO and 5% Cu-doped ZnO appeared light brown and dark brown, respectively (Fig. 3e and f).

3.2 Powder X-Ray Diffraction Analysis

Powder X-ray diffraction (XRD) analysis was done to determine the phase purity and crystallite size of the NPs. The XRD patterns for all four compounds analyzed, i.e., undoped ZnO NPs, 1% Cu-doped ZnO NPs, 5% Cu-doped ZnO, and commercial ZnO (C-ZnO), are shown in Fig. 4. From the XRD results, the diffraction peaks of the undoped ZnO NPs, 1%, and 5% Cu-doped ZnO NPs matched well with C-ZnO, which has a hexagonal wurtzite structure with the peaks positioned at 2θ values ranging from 31.84°, 34.48°, 36.32°, 47.60°, 56.64°, 62.92°, 66.44°, 68.02°, 69.16°, 72.60°, and 77.02° [3, 4]. These peaks were indexed as (100), (002), (101), (102), (110), (103), (200), (112), (201), (004), and (202) *hkl* planes, respectively. In specific, the presence of intense peaks for the (100), (002), and (101) planes indicates highly crystalline and single-phase ZnO NPs.

XRD analysis of undoped ZnO NPs, 1%, and 5% Cu-doped ZnO showed well resolved patterns of ZnO with no impurity peaks present. All the four materials showed similar XRD patterns suggesting that Cu have been successfully incorporated into the structure of ZnO. The crystallite size of each ZnO NPs was calculated using the Scherrer formula [3, 4] where C-ZnO exhibited the largest size (4.60 nm) followed by 5% Cu-doped ZnO (3.82 nm), 1% Cu-doped ZnO (3.75 nm) and undoped ZnO (3.17 nm). From the results obtained, it showed that doping the ZnO with Cu increased the crystallite size of the NPs.

3.3 UV-Vis Diffuse Reflectance Spectroscopy Analysis

UV-vis diffuse reflectance spectroscopy (UV-vis DRS) analysis was carried out to determine the band gap energy (E_g) of the synthesized nanomaterials. Figure 5 shows the analysis result of the nanomaterials using DRS, within the wavelength range from 200 to 800 nm. Both the undoped ZnO and 1% Cu-doped ZnO NPs showed absorbance at 410 nm (Fig. 5b and c) while the 5% Cu-doped ZnO NPs displayed absorbance at 430 nm [4]. The higher percentage of Cu doping to ZnO NPs has shifted the absorption to a longer wavelength. The UV-vis absorption band of ZnO and 1% Cu-doped ZnO NPs obtained at 410 nm whereas 5% Cu-doped ZnO NPs showed absorption band at 430 nm indicates a red shift, due to the formation of Cu-doped ZnO NPs [21]. The calculated E_g from the UV-vis DRS analysis of all the synthesized ZnO NPs indicated that both undoped ZnO and 1% Cu-doped ZnO have the same E_g, i.e., 3.03 eV, which was higher than the E_g of the 5% Cu-doped ZnO: 2.73 eV. The E_g at respective wavelength was calculated by using the photon energy formula below [3, 4]:

$$E_g = \frac{hc}{\lambda} \quad (1)$$

where h is Plank's constant (6.626×10^{-34} Js), c is the speed of light (3.0×10^8 ms^{-1}), and λ is wavelength (nm).

3.4 Scanning Electron Microscopy and Energy-Dispersive X-Ray Spectroscopy Analysis

Scanning electron microscopy (SEM) and energy-dispersive X-ray spectroscopy (EDX) analyses were used to study the morphology of the synthesized nanomaterials and determine its particles size and also elemental composition. The SEM images taken at different magnification (× 50 000 and × 55 000) are displayed in Fig. 6. It showed that all the NPs, i.e.,

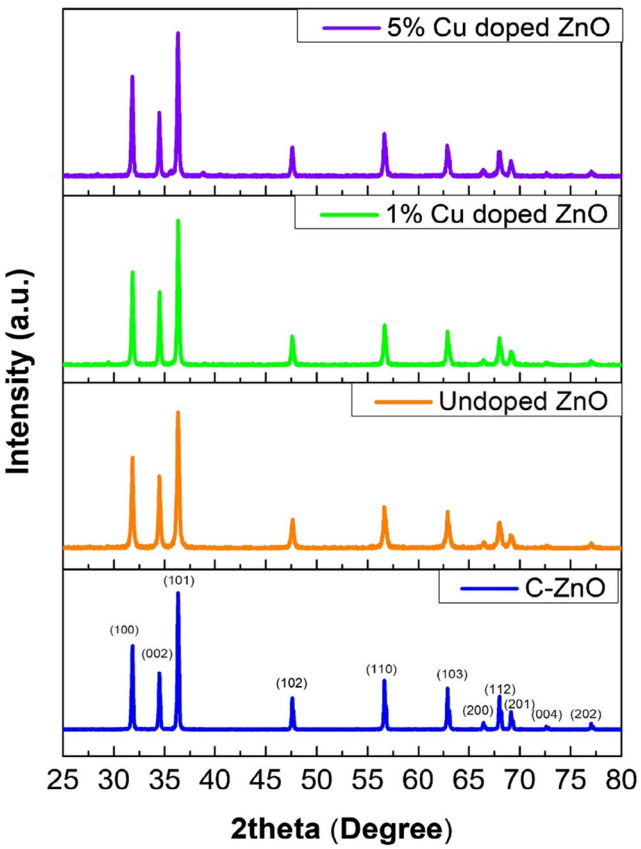

Fig. 4 Stacked XRD patterns for C-ZnO, undoped ZnO, 1% Cu-doped ZnO, and 5% Cu-doped ZnO NPs

undoped ZnO, 1%, and 5% Cu-doped ZnO NPs, have almost spherical shape, and aggregation can be seen at certain places for both Cu-doped ZnO NPs. The mean particle size of the undoped ZnO NPs was 48.35 nm while for 1% and 5% Cu-doped ZnO NPs were 14.97 nm and 13.42 nm, respectively. This suggests that doping Cu into ZnO can result in reduction in the particle size. The EDX analysis clearly confirmed the presence of zinc and oxygen in all three analyzed samples.

3.5 X-Ray Photoelectron Spectroscopy Analysis

X-ray photoelectron spectroscopy (XPS) analysis was carried out on 5% Cu-doped ZnO NPs to investigate its binding energy and elemental composition. Figure 7a shows the XPS spectra of survey 5% Cu-doped ZnO NPs with corresponding peaks assigned to Zn (2p), Cu (2p), O (1 s), and C (1 s). As shown in Fig. 7b, the Zn (2p) peaks were observed at 1023.65 eV and 1046.75 eV [4], whereas, Cu (2p) having four peaks at 934.85 eV, 943.55 eV, 955.25 eV, and 963.35 eV, respectively. From Fig. 7d, the binding energy of O (1 s) was at 532.25 eV and the peak of C (1 s) was at 284.35 eV (Fig. 7e). The XPS confirmed the presence of Cu on the surface of the synthesized ZnO NPs.

3.6 Zeta Potential Determination

The surface net charge of all the synthesized NPs was determined by zeta potential (ζ) analysis. The analysis was done in triplicate to determine the zeta potential, and then, their mean values were calculated. From the zeta potential analysis, it showed that the net surface charge of undoped ZnO NPs, 1% Cu-doped ZnO NPs, and 5% Cu-doped ZnO NPs was 26.63 ± 0.74 mV, 3.68 ± 1.11 mV, and 3.66 ± 2.82 mV, respectively. Zeta potential values that are higher than 30 mV, either positive or negative, will lead to monodispersity while zeta potential values lower than 5 mV can lead to agglomeration [26]. Hence, the higher the zeta potential, the higher the stability of the NPs, and so avoid aggregation. The analysis results showed that both Cu-doped ZnO NPs had zeta potential smaller than 5 mV; thus, aggregation can be seen at certain places.

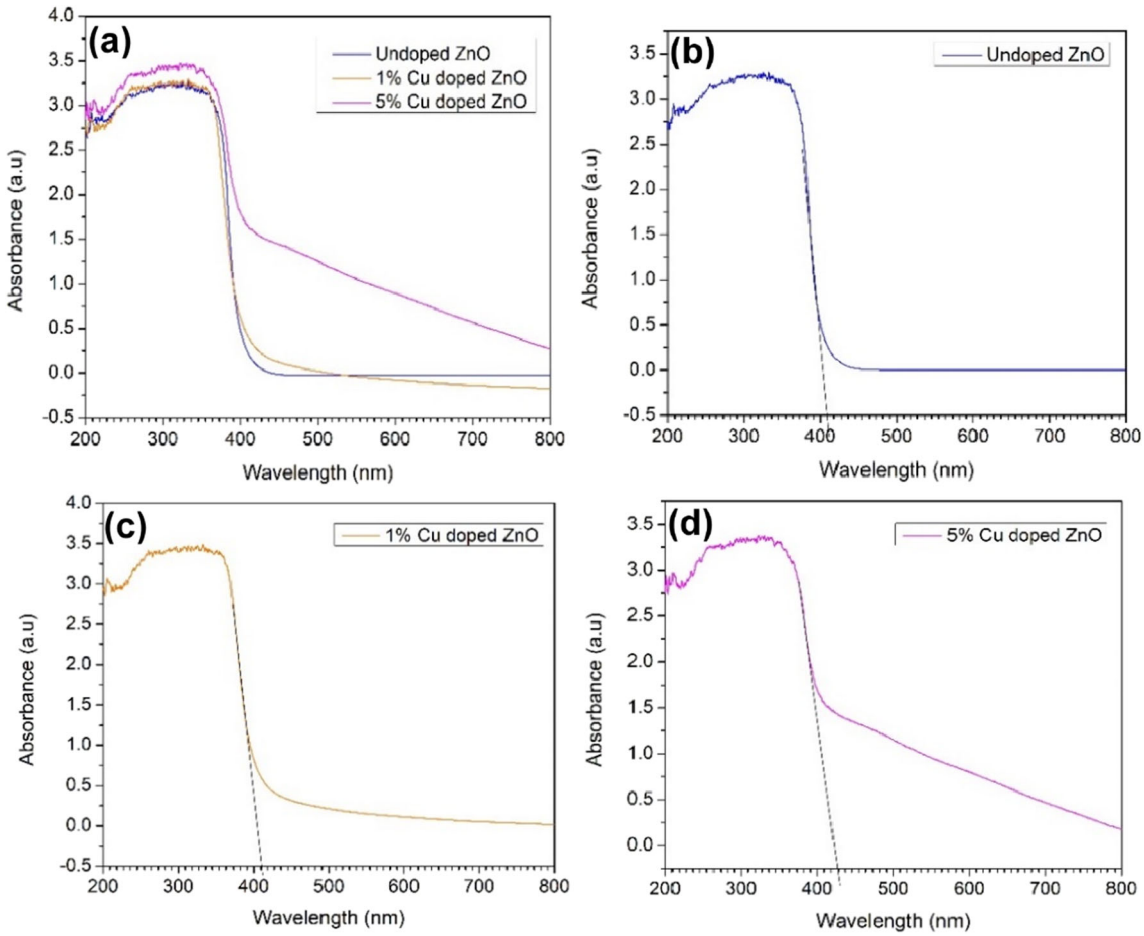

Fig. 5 **(a)** Overlapped DRS plot for undoped ZnO, 1% Cu-doped ZnO, and 5% Cu-doped ZnO, and DRS plot for (**b**) undoped ZnO, (**c**) 1% Cu-doped ZnO, and (**d**) 5% Cu-doped ZnO

3.7 Antibacterial Screening

The mean diameter of the inhibition zone for each of the five tested compounds is as shown in Table 1. It was observed that 5% Cu-doped ZnO exhibited the highest mean zone of inhibition followed by undoped ZnO, C-ZnO, and 1% Cu-doped ZnO for both *B.subtilis* and *S.aureus* tested. For the *S. aureus*, all the five compounds tested also demonstrated antibacterial activity as observed from the zone of inhibition on the bacterial growth. Similar to *B. subtilis*, 5% Cu-doped ZnO showed the largest zone of inhibition compared with the undoped ZnO, C-ZnO, and 1% Cu-doped ZnO (Table 1). The screening results obtained for both *P. aeruginosa* and *E. coli* have shown that there was no zone of inhibition detected for all four compounds tested at a concentration of 500 mg/mL.

The antibacterial screening results showed that the NPs were only able to inhibit the growth of gram-positive bacteria (*B. subtilis* and *S. aureus*) and not the gram-negative bacteria (*P. aeruginosa* and *E. coli*). Since gram-negative bacteria have a reduced amount of negatively charged peptidoglycan (between 3- and 20-fold), this has made it less susceptible to the positively charged antibacterial agents, Zn^{2+} ions from ZnO NPs [27]. The presence of the outer membrane in the gram-negative bacteria cell which contain lipopolysaccharide (LPS) acts as the protective barrier. The LPS will form a non-fluid continuum that can effectively block the hydrophobic molecules [18].

Gram-positive bacteria are less susceptible to the toxicity effect and the bactericidal effect of the ZnO NPs when compared with the gram-negative bacteria. This could be attributed to the presence of teichoic acid and lipoteichoic acid on the gram-positive bacteria that help chelate the Zn^{2+} ion from the ZnO NPs across cell membrane [8].

3.8 Minimum Inhibitory Concentration

Figure 8a shows the plates following the MIC tests with different concentrations of undoped ZnO NPs against *B. subtilis* while Fig. 8b and c show the tests for 1% and 5% Cu-doped ZnO, respectively. The inhibition zones indicate that the 5% Cu-doped ZnO was able to actively cause a higher bacterial inhibition for *B. subtilis*.

Similarly, Fig. 9a shows the plates following the MIC tests with different concentrations of undoped ZnO NPs against *S. aureus* while Fig. 9b and c show the tests for 1% and 5% Cu-doped ZnO, respectively. The inhibition zones indicate that the 5% Cu-doped ZnO was able to actively cause a higher bacterial inhibition for *S. aureus*.

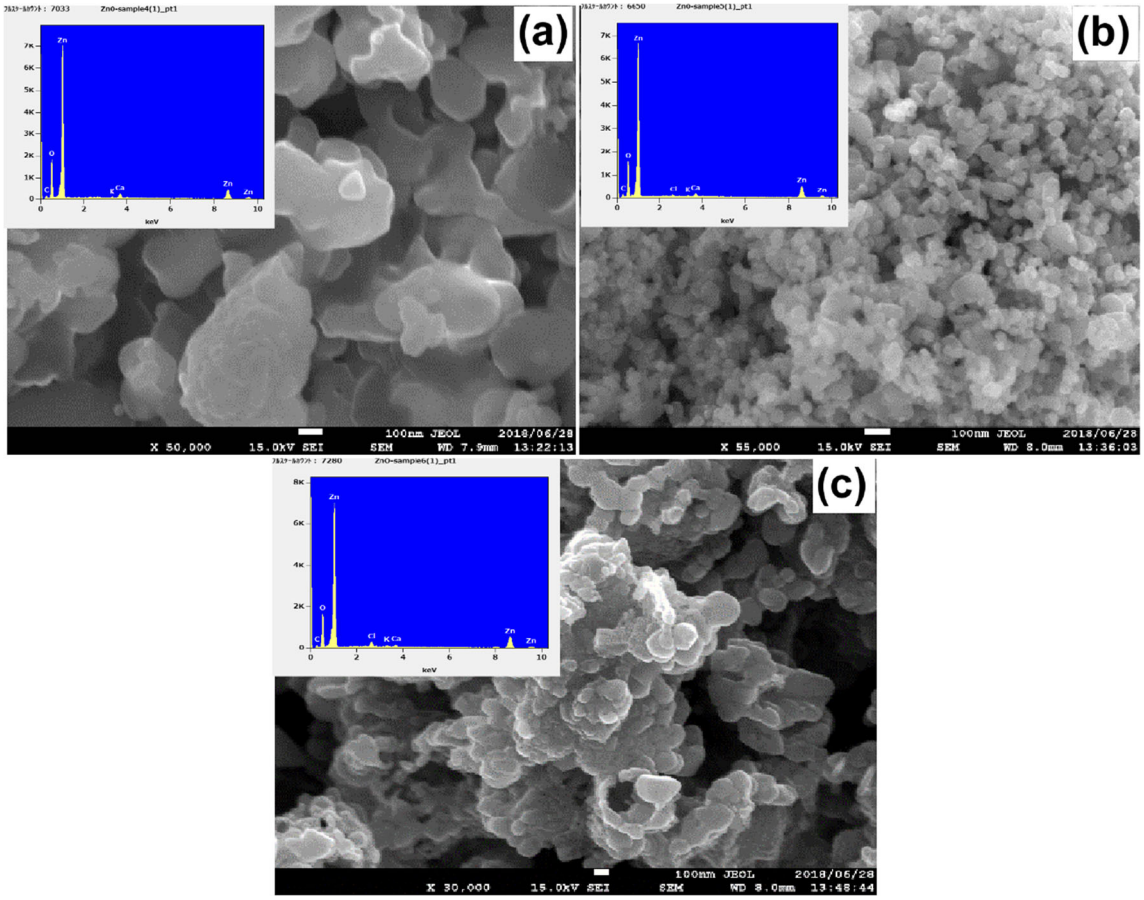

Fig. 6 SEM images of (**a**) undoped ZnO, (**b**) 1% Cu-doped ZnO, and (**c**) 5% Cu-doped ZnO and inset shows respective EDX spectra

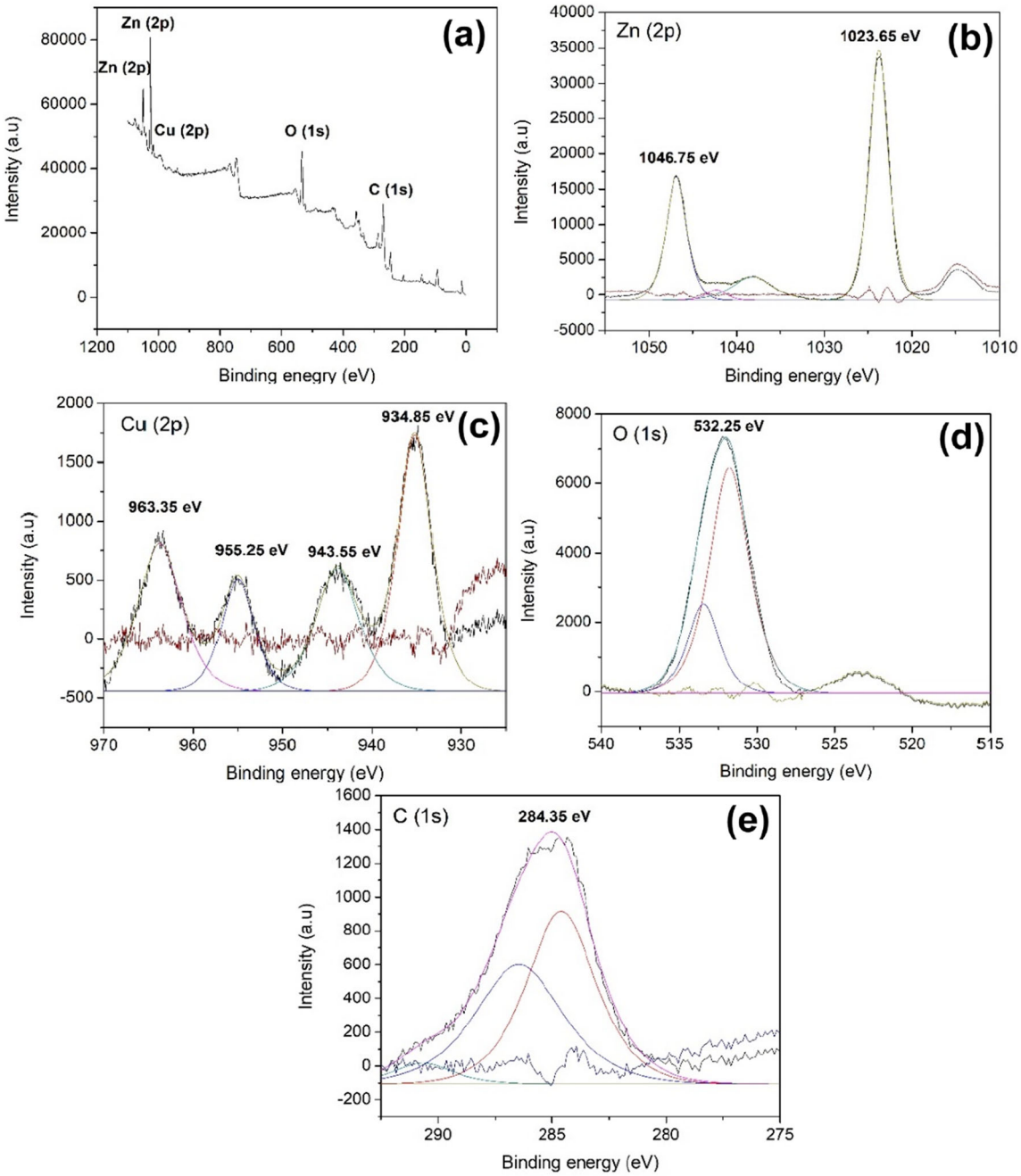

Fig. 7 XPS fitting spectra of 5% Cu-doped ZnO NPs, (**a**) survey, (**b**) Zn (2p), (**c**) Cu (2p), (**d**) O (1 s), and (**e**) C (1 s)

Table 1 Antimicrobial screening of NPs (500 mg/mL) against bacterial strains. Data are mean of three replicates ($n = 3$) ± SD

	Inhibition zone (mm)			
	Gram-positive bacteria		Gram-negative bacteria	
	B. subtilis	*S. aureus*	*E. coli*	*P. aeruginosa*
Undoped ZnO	12 ± 0.10	11 ± 0.0	0.0 ± 0.0	0.0 ± 0.0
1% Cu-doped ZnO	9.3 ± 0.06	9.3 ± 0.06	0.0 ± 0.0	0.0 ± 0.0
5% Cu-doped ZnO	14.3 ± 0.06	14.7 ± 0.06	0.0 ± 0.0	0.0 ± 0.0
C-ZnO	11 ± 0.0	10.3 ± 0.06	0.0 ± 0.0	0.0 ± 0.0
Streptomycin (20 mg/mL)	39.7 ± 0.06	25 ± 0.0	0.0 ± 0.0	0.0 ± 0.0

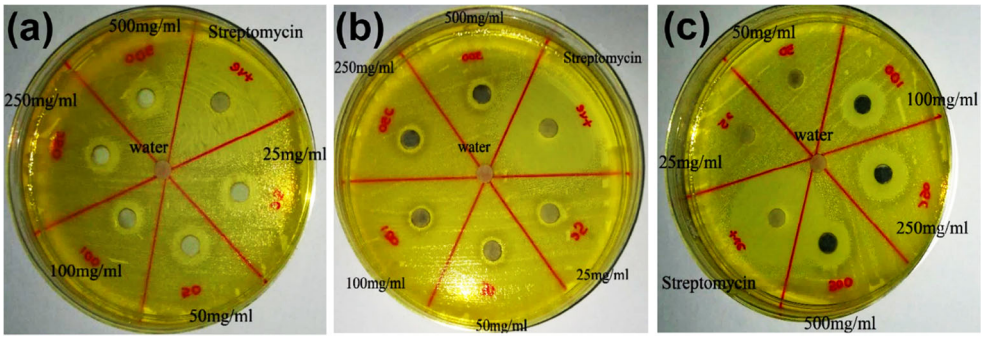

Fig. 8 Minimum inhibitory concentration (MIC) plates of different concentrations of (**a**) undoped ZnO, (**b**) 1% Cu-doped ZnO, and (**c**) 5% Cu-doped ZnO against *B. subtilis* growth, plates include streptomycin as positive control and distilled water as negative control

The mean diameters of the inhibition zones for *B. subtilis* and *S. aureus* are recorded in Table 2. The largest diameter recorded was from 250 mg/mL concentration of the 5% Cu-doped ZnO (14.3 mm). The MIC figures indicate high antibacterial activity observed for the different nanoparticles as evident from the MIC values which falls below 25 mg/mL tested (Table 2).

Figure 10a and b shows the mean diameter of the zone of inhibition for the growth of *B. subtilis* and *S. aureus* at different concentrations of the administered ZnO NPs. There was a significant difference ($p < 0.05$) between all three synthesized ZnO NPs (undoped ZnO, 1%, and 5% Cu-doped ZnO) and streptomycin for both *B. subtilis* and *S. aureus* at the highest concentration of ZnO NPs used at 500 mg/mL. For *B. subtilis*, there was a significant difference between undoped ZnO NPs and 5% Cu-doped ZnO NPs ($p < 0.05$) as well as between 1% Cu-doped ZnO NPs and 5% Cu-doped ZnO NPs ($p < 0.05$) with an increase in the inhibitory activity observed as the concentration of the ZnO NP increases. These findings suggest that a higher doping percentage increased the bactericidal effect of the Cu-doped ZnO NPs, and this effect was seen as dose dependent for the 5% Cu-doped ZnO. In the current study, results have shown that the mean particle size of the undoped ZnO NPs was 48.35 nm while for 1% and 5% Cu-doped ZnO NPs were 14.97 nm and 13.42 nm, clearly indicating a reduction in the size. Previous studies have reported that a decrease in the size of the particles increases the surface to volume ratio, and therefore increases bactericidal activity due to enhanced binding forces and the generation of free radicals within the cell which could contribute to our observed result [28].

As for *S. aureus*, there was no significant difference ($p > 0.05$) between all three synthesized ZnO NPs when compared with the undoped ZnO, indicating that doping ZnO NPs with Cu did not enhance the antibacterial activity of the undoped ZnO and that increasing the doping percentage did not result in an increased bactericidal effect of the Cu-doped ZnO. The Cu-doped ZnO did not show an enhanced antibactericidal effect indicating the doping did not increase the mechanism of antibacterial effect of NPs attributed to the major processes such as disruption of bacterial cell membrane, reactive oxygen species (ROS) generation, penetration of bacterial cell membrane, and induction of intracellular antibacterial effects involving the interactions with DNA and proteins [29, 30]. The lack of significant relationship observed in the doped vs undoped ZnO could also be attributable to the lack of a low enough concentration of doped vs undoped ZnO that can clearly distinguish the antibacterial activities. The emergence of increased bacterial resistance is of concern in recent years. Antibacterial mechanism of various nanoparticles involves at least one of the mechanisms of alteration of membrane permeability, generation of reactive oxygen species (ROS), enzyme inhibition, reduced DNA production, disruption of energy transduction, and photocatalysis [31]. Further elucidation on these different parameters will need to be investigated in order to determine the exact mechanism of antibacterial activity as observed in *B. subtilis* and *S. aureus*.

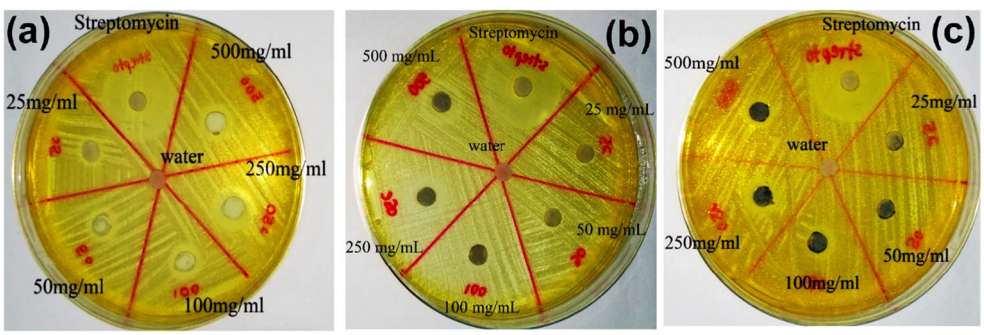

Fig. 9 MIC plates of different concentrations of (**a**) undoped ZnO, (**b**) 1% Cu-doped ZnO, and (**c**) 5% Cu-doped ZnO against *S. aureus* growth, plates include streptomycin as positive control and distilled water as negative control

Table 2 Mean diameter (± SD) of the respective zone of inhibition on the growth of *B. subtilis* and *S. aureus* against different concentrations of undoped ZnO and 1% Cu-doped and 5% Cu-doped ZnO

Concentration of NPs	Undoped ZnO	1% Cu-doped ZnO	5% Cu-doped ZnO
B. subtilis inhibition zone (mm)			
20 mg/mL streptomycin	38.3 ± 0.15	40.0 ± 0.10	39.3 ± 0.12
500 mg/mL	11.7 ± 0.06	9.7 ± 0.06	15.0 ± 0.0
250 mg/mL	11.0 ± 0.0	8.7 ± 0.06	14.3 ± 0.06
100 mg/mL	10.0 ± 0.0	8.0 ± 0.10	13.7 ± 0.06
50 mg/mL	11.0 ± 0.0	7.7 ± 0.06	6.0 ± 0.0
25 mg/mL	9.7 ± 0.06	8.0 ± 0.0	5.0 ± 0.0
MIC values	< 25 mg/mL	< 25 mg/mL	50 mg/mL
S. aureus inhibition zone (mm)			
500 mg/mL	10.7 ± 0.06	8.3 ± 0.23	8.7 ± 0.12
250 mg/mL	11.3 ± 0.06	8.7 ± 0.29	10.3 ± 0.25
100 mg/mL	10.0 ± 0.10	6.7 ± 0.12	6.7 ± 0.12
50 mg/mL	9.0 ± 0.10	6.3 ± 0.06	7.7 ± 0.12
25 mg/mL	8.0 ± 0.00	5.8 ± 0.06	6.7 ± 0.12
MIC values	< 25 mg/mL	< 25 mg/mL	< 25 mg/mL

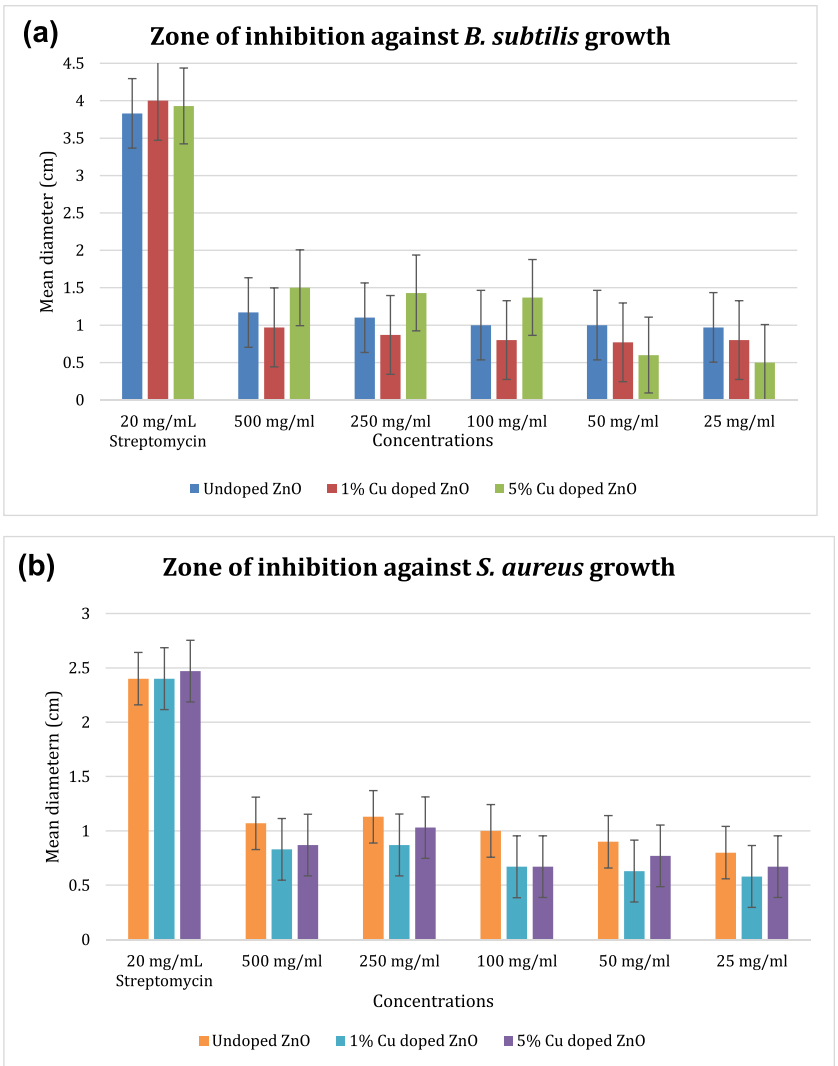

Fig. 10 Mean diameter of the zone of inhibition (cm) of the growth of (**a**) *B. subtilis* and (**b**) *S. aureus* tested at different concentrations of undoped ZnO and (1% and 5%) Cu-doped ZnO

4 Conclusion

This study reported a simple, phytogenic, eco-friendly, and cost-effective green method to synthesize ZnO NPs and (1% and 5%) Cu-doped ZnO NPs using aqueous leaf extract of *S. jamaicensis*. The structure, crystallite size, morphology, and composition of the ZnO, 1% Cu-doped ZnO, and 5% Cu-doped ZnO were confirmed through XRD, SEM-EDX, and XPS. The antibacterial screening results revealed that the green synthesized undoped ZnO NPs and both Cu-doped ZnO NPs had a noteworthy inhibition of growth against gram-positive bacteria only, i.e., *B. subtilis* and *S. aureus* but not against the gram-negative bacteria *P. aeruginosa* and *E. coli*. Hence, both gram-positive bacteria were preceded for MIC testing at different concentrations of the undoped and Cu-doped ZnO NPs. The results showed that both the undoped ZnO NPs and Cu-doped ZnO NPs exhibited the largest zone of inhibition against *B. subtilis* at 500 mg/mL with undoped ZnO followed by 1% Cu-doped ZnO and 5% Cu-doped ZnO. For *S. aureus*, the largest zone of inhibition was recorded at 250 mg/mL undoped ZnO followed by 1% Cu-doped ZnO and 5% Cu-doped ZnO. Our study showed that the three different NPs tested had different antibacterial activities and could be explored further for its application in healthcare and biotechnological applications.

Acknowledgments Authors would like to acknowledge the FIC grant UBD/RSCH/1.4/FICBF(b)/2018/012 from Universiti Brunei Darussalam, Brunei Darussalam.

References

1. Ansari, S. A., Khan, M. M., Kalathil, S., Nisar, A., Lee, J., & Cho, M. H. (2013). Oxygen vacancy induced band gap narrowing of ZnO nanostructure by electrochemically active biofilm. *Nanoscale, 5*, 9238–9246. https://doi.org/10.1039/c3nr02678g.
2. Kennedy, J., Murmu, P. P., Manikandan, E., & Lee, S. Y. (2014). Investigation of structural and photoluminescence properties of gas and metal ions doped zinc oxide single crystals. *Journal of Alloys and Compounds, 616*, 614–617. https://doi.org/10.1016/j.jallcom.2014.07.179.
3. Khan, M. M., Saadah, N. H., Khan, M. E., Harunsani, M. H., Tan, A. L., & Cho, M. H. (2019). Phytogenic synthesis of band gap-narrowed ZnO nanoparticles using the bulb extract of Costus woodsonii. *Bionanoscience, 9*, 334–344. https://doi.org/10.1007/s12668-019-00616-0.
4. Khan, M. M., Saadah, N. H., Khan, M. E., Harunsani, M. H., Tan, A. L., & Cho, M. H. (2019). Potentials of Costus woodsonii leaf extract in producing narrow band gap ZnO nanoparticles. *Materials Science in Semiconductor Processing, 91*, 194–200. https://doi.org/10.1016/j.mssp.2018.11.030.
5. Makarov, V. V., Love, A. J., Sinitsyna, O. V., Makarova, S. S., Yaminsky, I. V., Taliansky, M. E., & Kalinina, N. O. (2014). "Green" nanotechnologies: synthesis of metal nanoparticles using plants. *Acta Naturae, 6*, 35–44 https://www.ncbi.nlm.nih.gov/pubmed/24772325.
6. Yuvakkumar, R., Suresh, J., & Hong, S. I. (2014). Green synthesis of zinc oxide nanoparticles. *Advances in Materials Research, 952*, 137–140. https://doi.org/10.4028/www.scientific.net/AMR.952.137.
7. Gunalan, S., Sivaraj, R., & Rajendran, V. (2012). Green synthesized ZnO nanoparticles against bacterial and fungal pathogens. *Progress in Natural Science: Materials International, 22*, 693–700. https://doi.org/10.1016/j.pnsc.2012.11.015.
8. Happy, A., Menon, S., Venkat Kumar, S., & Rajeshkumar, S. (2018). Mechanistic study on antibacterial action of zinc oxide nanoparticles synthesized using green route. *Chemico-Biological Interactions, 286*, 60–70. https://doi.org/10.1016/j.cbi.2018.03.008.
9. Černík, M., Thekkae Padil, V.V. (2013). Green synthesis of copper oxide nanoparticles using gum karaya as a biotemplate and their antibacterial application, *International Journal of Nanomedicine* 889. doi:https://doi.org/10.2147/IJN.S40599.
10. Ajitha, B., Kumar Reddy, Y. A., Reddy, P. S., Jeon, H. J., & Ahn, C. W. (2016). Role of capping agents in controlling silver nanoparticles size, antibacterial activity and potential application as optical hydrogen peroxide sensor. *RSC Advances, 6*, 36171–36179. https://doi.org/10.1039/c6ra03766f.
11. Liew, P.M., Yong, Y.K. (2016). *Stachytarpheta jamaicensis* (L.) Vahl: from traditional usage to pharmacological evidence, evidence-based complement. *Evidence-Based Complementary and Alternative Medicine* 2016. doi:https://doi.org/10.1155/2016/7842340.
12. Ezenwa, K. C., Ighodaro, I., & Macdonald, I. (2015). Antidiabetic activity of methanol extract of stachytarpheta jamaicensis in streptozotocin-induced diabetic rats. *Nigerian Journal of Pharmaceutical Sciences, 14*, 9–18.
13. Pandian, C., Srinivasan, A., & Pelapolu, I. C. (2013). Evaluation of wound healing activity of hydroalcoholic extract of leaves of Stachytarpheta jamaicensis in streptozotocin induced diabetic rats. *Der Pharmacia Lettre., 5*, 193–200.
14. Putera, K.A.S.I., Hamdan, S., Dan Biokejuruteraan, F.B. (2010). Antimicrobial activity and cytotoxic effects of *Stachytarpheta jamaicensis* (L), Vahl Crude Plant Extracts, *Universiti Teknologi Malaysia*. https://books.google.com.bn/books?id=7j9nnQAACAAJ.
15. Murugan, M., Murugan, T., & Wins, J. A. (2013). Antimicrobial activity and phytochemical constituents of leaf extracts of Cassia auriculata. *Indian Journal of Pharmaceutical Sciences, 75*, 122. https://doi.org/10.4103/0250-474X.113546.
16. Mitchell, G. J., Wiesenfeld, K., Nelson, D. C., & Weitz, J. S. (2013). Critical cell wall hole size for lysis in gram-positive bacteria. *Journal of The Royal Society Interface, 10*, 20120892. https://doi.org/10.1098/rsif.2012.0892.
17. Dizaj, S. M., Lotfipour, F., Barzegar-Jalali, M., Zarrintan, M. H., & Adibkia, K. (2014). Antimicrobial activity of the metals and metal oxide nanoparticles. *Materials Science and Engineering: C, 44*, 278–284. https://doi.org/10.1016/j.msec.2014.08.031.
18. Silhavy, T. J., Kahne, D., & Walker, S. (2010). The bacterial cell envelope. *Cold Spring Harbor Perspectives in Biology, 2*, a000414. https://doi.org/10.1101/cshperspect.a000414.
19. Shannon, R. D. (1976). Revised effective ionic radii and systematic studies of interatomic distances in halides and chalcogenides. *Acta Crystallographica Section A, 32*, 751–767. https://doi.org/10.1107/S0567739476001551.
20. Banu Bahşi, Z., & Oral, A. Y. (2007). Effects of Mn and Cu doping on the microstructures and optical properties of sol-gel derived ZnO thin films. *Optical Materials, 29*, 672–678. https://doi.org/10.1016/j.optmat.2005.11.016.
21. Robak, E., Coy, E., Kotkowiak, M., Jurga, S., Załęski, K., & Drozdowski, H. (2016). The effect of Cu doping on the mechanical and optical properties of zinc oxide nanowires synthesized by

hydrothermal route. *Nanotechnology, 27*, 175706. https://doi.org/10.1088/0957-4484/27/17/175706.

22. Herng, T. S., Lau, S. P., Yu, S. F., Yang, H. Y., Wang, L., Tanemura, M., & Chen, J. S. (2007). Magnetic anisotropy in the ferromagnetic Cu-doped ZnO nanoneedles. *Applied Physics Letters, 90*, 032509. https://doi.org/10.1063/1.2433028.
23. Yugandhar, P., Vasavi, T., Uma Maheswari Devi, P., & Savithramma, N. (2017). Bioinspired green synthesis of copper oxide nanoparticles from Syzygium alternifolium (Wt.) Walp: characterization and evaluation of its synergistic antimicrobial and anticancer activity. *Applied Nanoscience, 7*, 417–427. https://doi.org/10.1007/s13204-017-0584-9.
24. Shanmugam, V., & Jeyaperumal, K. S. (2018). Investigations of visible light driven Sn and Cu doped ZnO hybrid nanoparticles for photocatalytic performance and antibacterial activity. *Applied Surface Science, 449*, 617–630. https://doi.org/10.1016/j.apsusc.2017.11.167.
25. Bauer, A. W., Kirby, W. M., Sherris, J. C., & Turck, M. (1966). Antibiotic susceptibility testing by a standardized single disk method. *American Journal of Clinical Pathology, 45*, 493–496. https://doi.org/10.1093/ajcp/45.4_ts.493.
26. Gumustas, M., Sengel-Turk, C.T., Gumustas, A., Ozkan, S.A., Uslu, B. (2017). Effect of polymer-based nanoparticles on the assay of antimicrobial drug delivery systems, in: Multifunct. Syst. Comb. Deliv. Biosensing Diagnostics, Elsevier: pp. 67–108. doi:https://doi.org/10.1016/B978-0-323-52725-5.00005-8.
27. Ren, G., Hu, D., Cheng, E. W., Vargas-Reus, M. A., Reip, P., & Allaker, R. P. (2009). Characterisation of copper oxide NPs for antimicrobial applications. *International Journal of Antimicrobial Agents, 33*(6), 587–590. https://doi.org/10.1016/j.ijantimicag.2008.12.004.
28. Oves, M., Arshad, M., Khan, M. S., Ahmed, A. S., Azam, A., & Ismail, I. M. I. (2015). Anti-microbial activity of cobalt doped zinc oxide nanoparticles: Targeting water borne bacteria. *Journal of Saudi Chemical Society, 19*(5), 581–588. https://doi.org/10.1016/j.jscs.2015.05.003.
29. Wang, L., Hu, C., & Shao, L. (2017). The antimicrobial activity of nanoparticles: present situation and prospects for the future. *International Journal of Nanomedicine, 12*, 1227–1249. https://doi.org/10.2147/IJN.S121956.
30. Khan, M. M., Harunsani, M. H., Tan, A. L., Hojamberdiev, M., Azamay, S., & Ahmad, N. (2020). Antibacterial activities of zinc oxide and Mn-doped zinc oxide synthesized using *Melastoma malabathricum* (L.) leaf extract. *Bioprocess and Biosystems Engineering, 43*(8), 1499–1508. https://doi.org/10.1007/s00449-020-02343-3.
31. Shaikh, S., Nazam, N., Rizvi, S. M. D., Ahmad, K., Baig, M. H., Lee, E. J., & Choi, I. (2019). Mechanistic insights into the antimicrobial actions of metallic nanoparticles and their implications for multidrug resistance. *International Journal of Molecular Sciences, 20*(10), 2468. https://doi.org/10.3390/ijms20102468.